Biosensors and Bioelectronics 142 (2019) 111519

Contents lists available at ScienceDirect

Biosensors and Bioelectronics

journal homepage: www.elsevier.com/locate/bios

Rhinophore bio-inspired stretchable and programmable electrochemical sensor

Shuqi Wang[a], Chunyan Qu[a], Lin Liu[b], Lianhui Li[a], Tie Li[a], Sujie Qin[b], Ting Zhang[a,*]

[a] i-Lab, and Key Laboratory of Multifunctional Nanomaterials and Smart Systems, Suzhou Institute of Nano-Tech and Nano-Bionics (SINANO), Chinese Academy of Sciences (CAS), 398 Ruoshui Road, Suzhou, Jiangsu, 215123, PR China

[b] Xi'an Jiaotong Liverpool University, Department of Environmental Science, 111 Renai Road, Suzhou, Jiangsu, 215123, PR China

ARTICLE INFO

Keywords:
Stretchable sensor
Rhinophore
Bio-inspired
Glucose sensor
Programmable sensitivity

ABSTRACT

Rhinophore, a bio-chemical sensory organ with soft and stretchable/retractable features in many marine molluscs species, exhibits tunable chemosensory abilities in terms of far/near-field chemical detection and molecules' source orientation. However, existing artificial bio-chemical sensors cannot provide tunable modality sensing. Inspired by the anatomical units (folded sensory epithelium) and the functions of a rhinophore, this work introduces a stretchable electrochemical sensor that offers a programmable electro-catalytic performance towards glucose based on the fold/unfold regulation of the gold nanomembrane on an elastic fiber. Geometrical design rationale and covalent bonding strategy are used to realize the robust mechanical and electrical stability of this stretchable bionic sensor. Electrochemical tests demonstrated that the sensitivities of the as-prepared bionic sensor exhibit a linear relationship with its strain states from 0% to 150%. Bio-inspired sensory functions are tested by regulating the strain of the bionic sensor. The sensor achieves a sensitivity of 195.4 $\mu A\,mM^{-1}$ in a low glucose concentration range of 8–206 μM at 150% strain for potentially far-field chemical detection, and a sensitivity of 14.2 $\mu A\,mM^{-1}$ in a high concentration range of 10–100 mM at 0% strain for near-field chemical detection. Moreover, the bionic sensor performs the detection while extending its length can largely enhance the response signal, which is used to distinguish the molecules' source direction. This proposed bionic sensor can be useful in wearable devices, robotics and bionics applications which require diverse modality sensing and smart chemical tracking system.

1. Introduction

In sea, animals are more dependent upon chemical information than vision (Cummins et al., 2009). Marine molluscs track food source or sense predator's odor in water by using a soft and stretchable/retractable olfactory organ named as rhinophore in *Aplysia*, *Nautilus*, *Nudibranchs,* et al. (Atema, 2018; Cummins et al., 2009; Ruth et al., 2002). Rhinophore is a tentacle commonly with folded epithelium which could enable bearing a high density of chemoreceptive cells (Basil et al., 2005). This naturalistic chemical sensor is structurally elaborate for tracking molecules by extending and retracting its length (Basil et al., 2000). The smart extending/retracting process endows animals with tunable chemical sensibility, which enables detecting lower concentration of molecules that far from the source with an extended state of the rhinophore, tracking along the direction of the greatest concentration from the food source with a moderate state, and setting a higher concentration response threshold with a retracted state for more abundant food (Atema, 2018). This tunable sensitivity is of great importance for animals to intelligently adjust their sense and tracking behavior in order to efficiently locate the food source and avoid energy expenditure. Inspiringly, a stretchable/retractable bio-chemical sensor with programmable sensitivity can detect molecules in a wide concentration range by conveniently adjusting its length, which is potentially useful in diverse smart systems such as wearable devices, robotics and bionics (Cai et al., 2017; Chen et al., 2017; Ristic et al., 2017; Yang et al., 2018).

Recently developed flexible and stretchable electronics provide several methods to attempt to fabricate and assemble an electrochemical sensor on the elastomeric substrate (Bandodkar et al., 2016a; Yang and Gao, 2018). Various nanomaterials and structures are designed to achieve the high stretchability, resistance stability as well as electrochemical activity (Heikenfeld et al., 2018). For example, one-dimensional carbon nanotubes (CNTs) (Abellán-Llobregat et al., 2017; Bandodkar et al. 2015, 2016b), gold nanowires networks (Liu et al.

* Corresponding author.
E-mail address: tzhang2009@sinano.ac.cn (T. Zhang).

https://doi.org/10.1016/j.bios.2019.111519
Received 7 May 2019; Received in revised form 28 June 2019; Accepted 15 July 2019
Available online 16 July 2019
0956-5663/

2016, 2017), graphene (Lee et al., 2016) and serpentine structural metal materials (Lee et al., 2017; Rogers, 2017) are assembled on silicone elastomers (such as polydimethylsiloxane (PDMS) and Ecoflex (Smooth-On)) via lithographic techniques, spin/spray coating methods and screen printing techniques, etc. However, their analytical performance such as sensitivity is still changeable in certain extent during stretching/retracting process due to the non-regulated electrical resistance and electrochemical surface active area (ECSA) (Jiang et al., 2018; Liu et al., 2016; Zhu and Moran-Mirabal, 2016). As is well known that ECSA is crucial for electrochemical sensor according to the Cottrell's relation (Windmiller and Wang, 2013). The fundamental consideration in design and operation of a flexible and stretchable electrochemical sensor is to preserve its electrode area or regulate it with the programmable sensitivities. On the contrary, the unstable electrical resistance and non-regulated electrochemical active area will have a direct impact on the transduced current, resulting with unexpected sensor performances. Therefore, rational design and control the ECSA is crucial for the development of the flexible and stretchable electrochemical sensor.

Nature gives the answer. As a naturalistic stretchable electrochemical sensor, rhinophore possesses a sophisticated sensory epithelium with folded surface area, an illustration of its anatomical units is presented in Fig. 1A and B. The folded epithelium bears a high density of sensory cells and exhibits transverse ridges and grooves that surround the rhinophore trunk (Cummins et al., 2009; Ruth et al., 2002). From functional perspective, in a retracted state of the rhinophore, some olfactory cells sunken between the ridges, this probably results in low chemical sensitivity because a relatively small sensory area exposure and more molecules need to diffuse to reach those sensory cells (Basil et al., 2005). Conversely, by extending of the rhinophore to increase the surface area, animals can detect lower concentration that far from the source. Inspired by this geometry and capacity, we designed a stretchable electrochemical sensor based on folded gold nanomembrane and demonstrated its programmable sensory ability along with the stretching/retracting feature. The key to realize this bionic similarity lies in the successful fabrication and regulation of the fold/unfold ECSA on a highly elastic Ecoflex fiber. With this approach, the as-prepared stretchable electrochemical sensor achieved a well tunable electrocatalytic performance towards glucose by adjusting the strain of the sensor from 0% to 150%. Particularly, the sensor can mimic the near-field (high concentration range) and far-field (low concentration range) chemical detection with different sensitivities at the retracted state (0%) and the extended state (150%), respectively. Furthermore, this bionic sensor in a stretching detecting mode (detecting while stretching the sensor) can greatly enhance the response signal and result with a basically distinguish function of the orientation to molecules' source in the ambient concentration gradient (analogous to odor plumes).

2. Material and methods

2.1. Reagents and materials

Gold chloride trihydrate ($HAuCl_4{\cdot}3H_2O$) and (3-mercaptopropyl) trimethoxysilane ($C_6H_{16}O_3SSi$, MPTS) were obtained from Sigma-Aldrich (Shanhai) Trading Co., Ltd. Glucose, potassium ferricyanide ($K_3Fe(CN)_6$), potassium ferrocyanide trihydrate ($K_4Fe(CN)_6{\cdot}3H_2O$) were obtained from Aladdin (Shanghai) Co., Ltd. Gold films (~200 nm in thickness) were purchased from Nanjing Gold Foil Group (Nanjing,

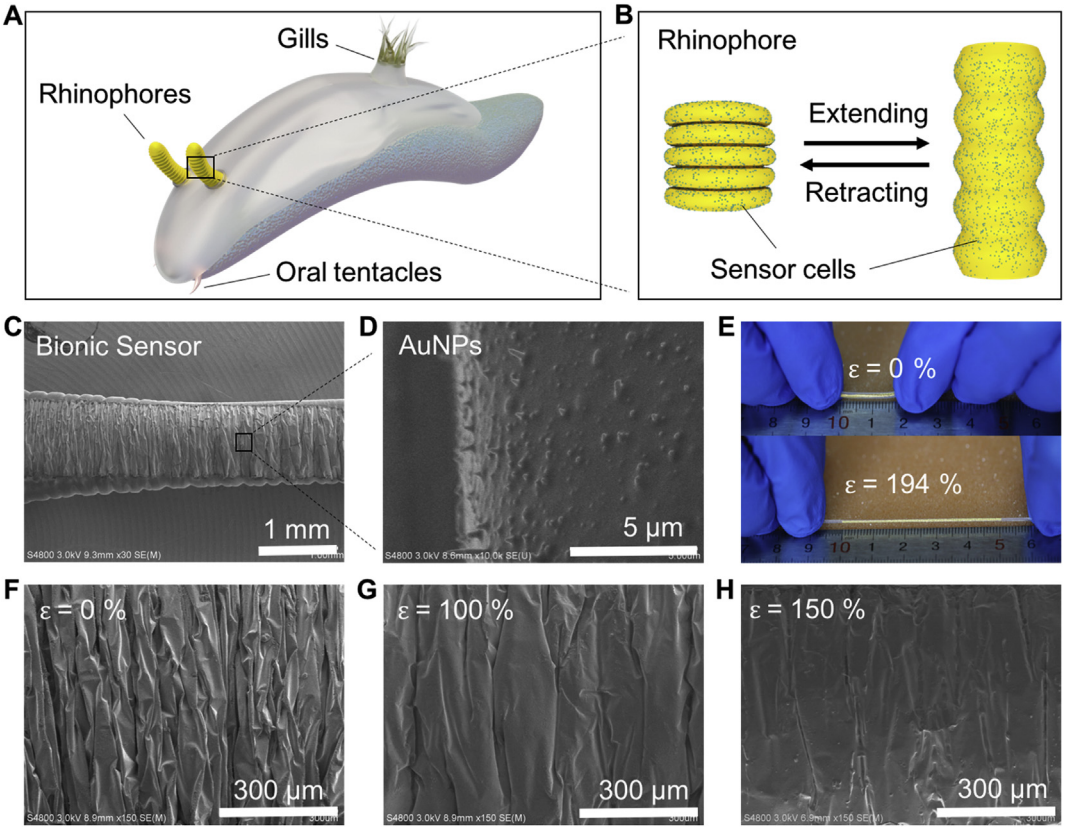

Fig. 1. Schematic illustrations and images of a stretchable electrochemical sensor based on the folded gold nanomembrane inspired by a marine mollusc's rhinophore. (A) Illustration of a dorid nudibranch species possesses a pair of rhinophore, oral tentacles and gills. (B) The enlarged illustration shows a rhinophore with numerous sensory cells scattered all over the epithelium at its extended and retracted state. (C) SEM images of a folded gold nanomembrane based stretchable bionic sensor. (D) SEM image of gold nanoparticles scattered all over the gold nanomembrane surface. (E) Optical image of the stretchable sensor at 0% and 194% strained state. (F) SEM images of the stretchable senor at 0%, (G) 100% and (H) 150% applied strain. (For interpretation of the references to colour in this figure legend, the reader is referred to the Web version of this article.)

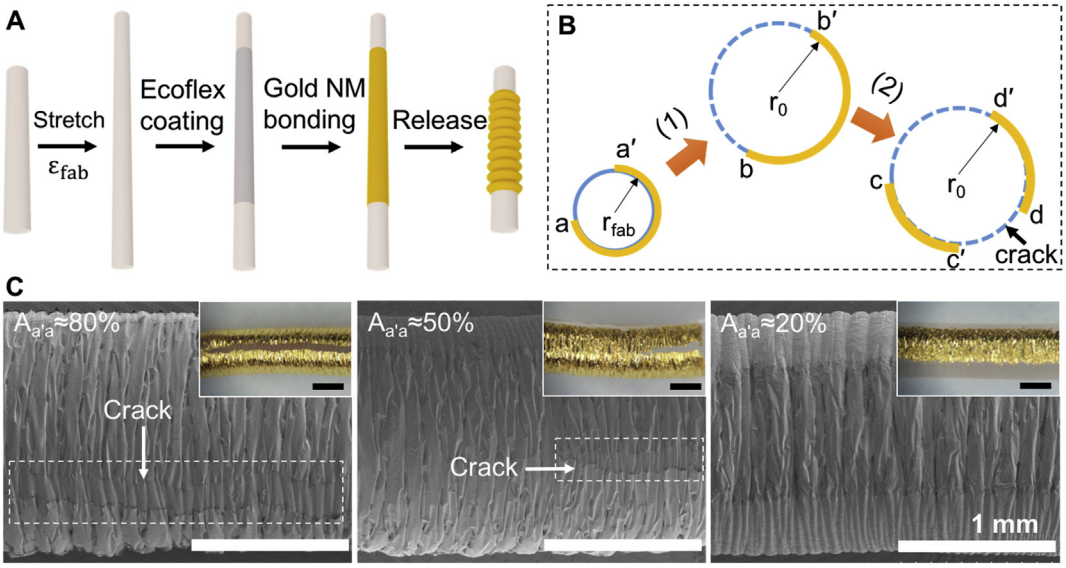

Fig. 2. Schematic illustrations of the stretchable bionic electrode fabrication process and the SEM and optical images of the cracks regulation. (A) The illustrations of the bionic electrode fabrication process. The pre-stretched strain denoted as ε_{fab}, gold NM refers to gold nanomembrane. (B) The illustrations of the cracks formation mechanism. (C) SEM and optical images of the stretchable bionic electrode fabricated with different W (equals to different $A_{a'a}$) in the relaxed state. All scale bars are 1 mm. (For interpretation of the references to colour in this figure legend, the reader is referred to the Web version of this article.)

China). Ecoflex™ 00–30 silicone rubber was obtained from Smooth-On, Inc. (Lower Macungie, PA). Hg/HgO (1.0 mol/L KOH) reference electrode was purchased from Shanghai Yueci Electronics Technology Co., Ltd. Ag/AgCl ink (product no.011464) for reference electrode was purchased from ALS (Japan) Co., Ltd. All other chemicals were commercially available and of analytical reagent grade. All reagents were used as received. The aqueous solutions were prepared freshly with deionized water (18.2 MΩ cm).

2.2. Stretchable bionic sensor fabrication

The electrode fabrication process is shown in Fig. 2A. The Ecoflex fiber of different diameters were fabricated by curing prepolymer in polytetrafluoroethylene (PTFE) tubes (with different diameters) and cutting out when needed. The gold nanomembrane (supported on paper substrate) was immersed in 10 mM MPTS toluene solution for 30 min and followed by a heat treatment at 150 °C in air for 1 h. Then the gold nanomembrane was cut into different sizes for use. The Ecoflex fiber was pre-stretched with a ε_{fab}, then Ecoflex prepolymer was sprayed over the fiber to form a thin layer of glue and waited for 20 min in air until half cured. The gold nanomembrane was attached on the Ecoflex fiber surface and waited for 2 h until the glue fully cured. Finally, the electrode was achieved by releasing the pre-stretched fiber. Connecting wires (Au wires, 0.06 mm in diameter) were bonded at each end of the gold nanomembrane. The gold nanoparticles on the surface of the electrode were fabricated by an electrodeposition method in 1 mg/mL $HAuCl_4$ (in 0.1 M KNO_3) versus a homemade Ag/AgCl reference electrode wire and a Pt wire counter electrode. The homemade Ag/AgCl reference electrode wire was made by coating a layer of Ag/AgCl ink and dry overnight.

2.3. Characterization

SEM images were characterized by using a field-emission scanning electron microscope (FE-SEM; Hitachi-s4800). Optical images were taken by a microscope (Motic SMZ-168). Electrical conductivities were measured by a Gamry Reference 600 + potentiostat using a two electrode setup.

2.4. Electrochemical measurements

All the electrochemical experiments were carried out in a custom-designed cell with three electrodes setup (Fig. S5A) using a Gamry Reference 600 + potentiostat. ECSA tests were carried out in 0.5 M H_2SO_4 solution. Electrochemical impedance spectroscopy (EIS) was performed in 5 mM $Fe(CN)_6^{3-/4-}$ with 0.1 M KCl solutions. CV measurements were carried out in different concentration of $Fe(CN)_6^{3-/4-}$ solutions vs. a homemade Ag/AgCl reference electrode wire. Glucose detection was carried out in 0.1 M NaOH electrolyte solution vs. a Hg/HgO (1.0 mol/L KOH) reference electrode.

3. Results and discussion

3.1. Stretchable bionic sensor design, fabrication and electrical performance

Fig. 1C shows a stretchable bionic sensor with a folded gold nanomembrane conformally sticking on an Ecoflex fiber substrate (about 1.5 mm in diameter). Numerous gold nanoparticles (100–500 nm in diameter) scatter all over the gold nanomembrane surface, as shown in Fig. 1D and Fig. S1. The folded gold nanomembrane as well as gold nanoparticles vividly mimic the anatomical units of the rhinophore's epithelium and sensory cells. Analogous to rhinophore, this bionic electrode can extend and retract in a large strain range (up to ~200%, Fig. 1E). During the extending process, the initially folded gold nanomembrane (Fig. 1F) is gradually stretching and unfolding to expose the hidden surface area between these ridges and concaves (Fig. 1G and H). Importantly, to design such a stretchable electrochemical sensor with stable electrical conductivity and controllable sensing properties, the electrode resistance and the surface active area must be controllably regulated within a certain range of strain.

Herein, by combining pre-stretching/releasing method with covalent bonding modification and geometrical design, we proposed an inexpensive and high-quality approach to design and fabricate this highly stretchable folded gold nanomembrane based electrode. The detailed fabrication process is described in Methods and shown in Fig. 2A. As is well known, the flat gold film on elastomer substrate is easy to form cracks with applied strain (Fig. S2A, commonly less than 5%) (Kang et al., 2014; Kim et al., 2011; Zhu and Moran-Mirabal, 2016). Structuralizing metal film into special configurations such as serpentine,

wavy, island-bridge and wrinkles has been widely used to achieve good flexibility and stretchability on elastomer substrate (Wang et al., 2017). Among those approaches, wrinkles on metal film formed by pre-stretching/releasing method are more attractive for fabricating the stretchable electrochemical electrode because of its simple and cost-effective process (comparing with photolithography techniques) as well as the stable conductivity and larger area coverage of active materials on the elastomer substrate. In present work, a commercial available freestanding gold nanomembrane (about 200 nm thickness, Fig. S2B) is readily fabricated on the pre-stretched Ecoflex fiber substrate, instead of using expensive sputtering or evaporation processes fabricated gold film. Significantly, a strong interface adhesion between the thin gold nanomembrane and the elastomer substrate is crucial for improving the mechanical stability of the system (Qi et al., 2015). Two approaches are used to enhance this interface adhesion strength: firstly, the gold nanomembrane was treated with (3-mercaptopropyl)trimethoxysilane ($C_6H_{16}O_3SSi$, MPTS) to covalently bond with Ecoflex fiber substrate; secondly, a layer of Ecoflex prepolymer was sprayed over the fiber, then the MPTS-treated gold nanomembrane was adhered to the pre-stretched fiber with half-cured Ecoflex prepolymer and followed with fully curing process (at room temperature for 2 h). The MPTS-treated gold nanomembrane is fully bonded to the Ecoflex fiber and shows conformal contact with the folded wrinkle structures on the fiber after stretch-released (Fig. S2D, E and F). Comparatively, the MPTS-untreated gold nanomembrane adhering to the fiber substrate only with the pre-polymer tends to form suspended wrinkles with partially bonding points after pre-stretching/releasing process (Fig. S2C). Obviously, this incompletely bonded structure is mainly due to the weak interface adhesion strength, which will lead to the further detachment of the gold nanomembrane and result in the unstable conductivity and mechanical failure of the electrode. Therefore, the covalent bonding modification is one key design rationale to ensure the mechanical integrity and realize the stable electrical conductivity and controllable sensing properties of the sensor, their electrical performances will be discussed in following section.

To avoid cracks formation is another key issue for the design of the stretchable bionic sensor with stable electrical conductivity. Cracks occur parallel to the stretch/release direction after releasing the gold nanomembrane wrapped pre-stretched Ecoflex fiber. The cracks formation mechanism is shown in Fig. 2B. In brief, a gold nanomembrane (with a width of W and a length of L_0) is wrapped on the pre-stretched Ecoflex fiber (the pre-stretched strain denoted as ε_{fab}). Due to the positive Poisson's ratio of the Ecoflex fiber (~0.5), during the relaxation of the pre-stretched fiber, the length of the fiber decreases, the compressive strain causes the wrinkles formation because of the modulus mismatch between the gold nanomembrane and the elastic fiber; while the diameter of the fiber increases, which induces a stretching strain along the perimeter direction on the wrapped gold nanomembrane. Apparently, this diameter-enlargement induced strain is the major factor to cause the cracks' formation, which is denoted as ε_{dia} and can be evaluated as Equation (1):

$$\varepsilon_{dia} = \Delta A = A_{a'a} - A_{b'b} = W(R_0 - R_{fab})/(\pi R_{fab} R_0) \quad (1)$$

where A is the coverage ratio of the gold nanomembrane towards fiber perimeter, calculated as $A = W/\pi R$; $A_{a'a}$ and $A_{b'b}$ corresponding to the coverage ratio of the gold nanomembrane on the stretched fiber and the released fiber, respectively (Fig. 2B); R_{fab} is the diameter of the stretched fiber, R_0 is the diameter of the released fiber. It can be seen from Equation (1) that the width (W) of the gold nanomembrane determines the applied ε_{dia} at a specific ε_{fab} (when the fabrication ε_{fab} is determined, R_{fab} and R_0 are constant). R_{fab} at different ε_{fab} was measured by an optical microscope (R_0 = 1.5, 1.0, 0.5 mm are used). The experiment sets $A_{a'a}$ as 80%, 50% and 20% to evaluate the values of $A_{b'b}$ and ε_{dia} (ΔA) at different ε_{fab}. As shown in Fig. S3A and Fig. 3A, with increases of ε_{fab}, $A_{b'b}$ decreases and ε_{dia} (ΔA) increases, and the fibers with different diameters have the similar change tendency. However, from Fig. 3A it can be apparently concluded that ε_{dia} for $A_{a'a}$ = 80% and $A_{a'a}$ = 50% are changed over 30% (~30%–~50%), which are much larger than that of $A_{a'a}$ = 20% (ε_{dia} < 10%). The results indicate that ε_{dia} applied on the gold nanomembrane can be reduced by decreasing of W (i.e., decreases of $A_{a'a}$ on a certain pre-stretched fiber), therefore, the cracks can possibly be reduced or disappeared.

To prove the above theoretical cracks-avoidance strategy, gold nanomembrane with different W were fabricated on the pre-stretched fiber under different prestrain (ε_{fab} = 100%, 200%, 300%, 400%, 500%). As shown in Fig. S4 and Fig. 2C, for the electrodes fabricated with $A_{a'a} \approx 80\%$, cracks with large width (100 μm–500 μm) form parallel to the stretch/release direction and totally break through the gold nanomembrane; cracks turn larger with the increases in ε_{fab}. For the electrodes fabricated with $A_{a'a} \approx 50\%$, cracks tend to form at the end of the gold nanomembrane and elongate with the increases in ε_{fab}. For the electrodes fabricated with $A_{a'a} \approx 20\%$, no crack forms in the whole range of ε_{fab}. These experimental results well demonstrate that the cracks can be reduced and avoided by decreasing of $A_{a'a}$, which is due to the decreases in W can significantly reduce the ε_{dia} applied on the wrapped gold nanomembrane along the perimeter direction. Surprisingly, in the case of no crack formation for the electrodes fabricated with $A_{a'a} \approx 20\%$, the ε_{dia} is less than 10% but apparently larger than the strain to form cracks on flat gold film/substrate system (Fig. S2A). This enhanced strain endurance of the gold nanomembrane might attribute to their folding wrinkles surface that can distribute a certain degree of the strain. In addition, the stretchability of the electrodes fabricated with $A_{a'a} \approx 20\%$ is greater than that of the electrodes fabricated with $A_{a'a} \approx 80\%$ and $A_{a'a} \approx 50\%$, as shown in Fig. 3D. This is due to the gold nanomembrane is conformally and tightly bonded with the fiber substrate, and more interface contact between the film and the substrate will cause fiber harder to retract.

The electrical conductivities of the stretchable electrodes with or without cracks vary greatly. The conductivities were measured by two-probe setup (with two gold wires connected at both ends of the stretchable electrode). As Fig. 3B shown, the stretchable electrodes fabricated with $A_{a'a} \approx 80\%$ and $A_{a'a} \approx 50\%$ have apparent resistance changes towards stretching/releasing cycles in the strain range (0%–152% and 0%–170%, respectively). Their relative resistance changes ($\Delta R/R_0$) are much larger than that of the stretchable electrodes fabricated with $A_{a'a} \approx 20\%$, while the strain range (0%–186%) applied in the experiment of the later one ($A_{a'a} \approx 20\%$) is wider than those of the two former conditions. Additionally, the repeated stretching/releasing cycles in the strain range from 0% to 100% were monitored (Fig. 3C). The stretchable electrodes with cracks ($A_{a'a} \approx 80\%$, $A_{a'a} \approx 50\%$) lose their electrical conductivities after 500 and 1000 cycles, respectively. While, the stretchable electrode with no crack ($A_{a'a} \approx 20\%$) shows no obvious resistance change even after 10000 cycles. This significant difference in the electrical stability is due to the existed cracks on the gold nanomembrane surface will develop larger and expand to break the conductive paths of the electrodes (Fig. S5A). In contrast, the stretchable electrode with no crack will remain integrity for a long term use (Figs. S5B and C).

The above geometrical optimized stretchable electrode ($A_{a'a} \approx 20\%$) exhibits small variation in resistance change. As shown in Fig. 3E, the relative resistance changes ($\Delta R/R_0$) towards stretching/releasing cycles is less than 20% for a strain up to 186%, $\Delta R/R_0$ < 10% for a strain up to 170%, and can achieve $\Delta R/R_0$ < 5% for a strain up to 150%. Moreover, the real-time monitoring of the resistance changes of the stretchable electrode upon different mechanical deformations is shown in Fig. 3F. During bending, shacking (~5 Hz), twisting with a tweezer and even dragging with fingers, the stretchable electrode shows a $\Delta R/R_0$ < 10%. The results further demonstrate that the as-prepared stretchable electrode with no crack possesses robust mechanical and electrical stability withstanding various deformations. This excellent performance indicates that the stretchable electrode can well control its resistance

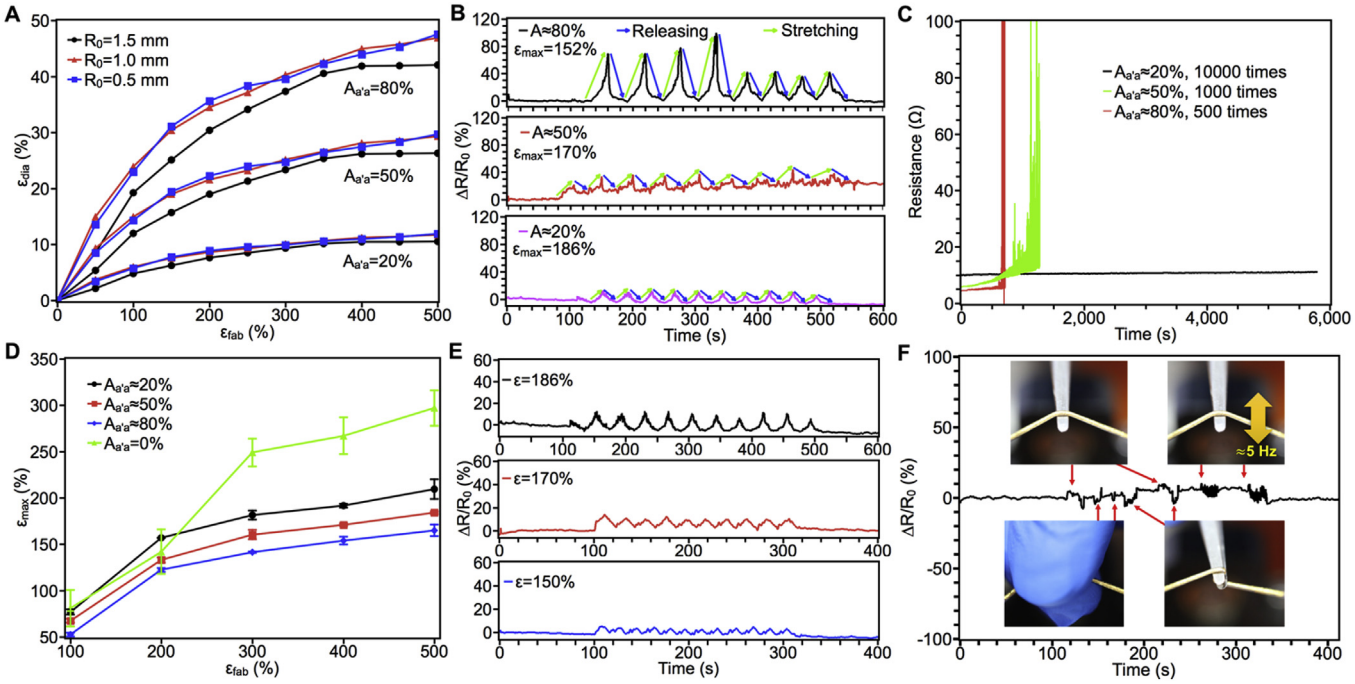

Fig. 3. The electrical performances of the stretchable bionic sensor. (A) The plots of ε_{dia} versus ε_{fab} for the stretchable electrode with different $A_{a'a}$ and R_0 given by Equation (1) and the measured R_{fab} values. (B) The real-time relative resistance changes ($\Delta R/R_0$) plots measured during stretching (green arrows) and releasing (blue arrows) of the stretchable electrode (fabricated with different $A_{a'a}$), ε_{max} refers to the maximum strain obtained after the stretched fiber released. (C) The resistance changes of the stretchable electrode (fabricated with different $A_{a'a}$) upon long term of stretching/releasing cycle from 0% to 100%. (D) The plots of ε_{max} versus ε_{fab} for the stretchable electrode (1.5 mm in diameter) with different $A_{a'a}$, ε_{max} refers to the maximum strain obtained after the stretched fiber released. (E) The real-time relative resistance changes plots for a stretchable electrode ($A_{a'a} \approx 20\%$) during stretching and releasing in different strain range. (F) The real-time relative resistance changes for the stretchable electrode measured upon different mechanical deformations, including bending, shacking (~5 Hz), twisting with a tweezer and dragging with fingers. (For interpretation of the references to colour in this figure legend, the reader is referred to the Web version of this article.)

change and the surface area integrity with high stretchability. Therefore, it is suitable for electrochemical sensing during mimic the extending/retracting process and function of rhinophore.

3.2. Programmable electrochemical performances of the stretchable bionic sensor

The as-prepared stretchable bionic sensor exposes tunable surface area by extending or retracting its folded gold nanomembrane (SEM images shown in Fig. 1F, G and H). Electrochemical active surface areas (ECSA) of the bionic sensor at different strain state were evaluated by cyclic voltammetry (CV) using a custom-designed cell with three electrodes setup (Fig. S6A). As shown in Fig. 4A, CV curves exhibit well-defined oxidation/reduction peaks of the gold surface atoms. With the increases in the strain of the sensor, the reduction peaks' current gradually increases. It is well known that ECSA is associated with the integrated charge transfer of the reduction peaks, which assuming 390 μC/cm^2 for a monolayer gold surface atom reduction, the ECSA is calculated as 0.42 cm^2, 0.50 cm^2, 0.62 cm^2 and 0.67 cm^2 for the strain of 0%, 50%, 100% and 150%, respectively. The results indicate that the stretchable bionic sensor can regulate the ECSA by controlling the extending and retracting state to tune the surface morphologies among fully folded to unfolded of the gold nanomembrane (illustrations inset in Fig. 4A).

EIS experiments were carried out to analyze the interfacial properties of the bionic sensor at different strain states. A typical impedance spectrum (Nyquist plot) includes a semicircle at high frequency and a straight line in the low frequency. The semicircle diameter corresponds to the electron-transfer resistance (R_{et}), and the linear part corresponds to the diffusion limited process. The Nyquist plots were shown in Fig. S7, the bionic sensor at different strain states exhibited similar spectrum of an ~45° Warburg diffusion line in the measured frequency range. The almost absence of the high-frequency semicircle indicates the fast electron transfer kinetics. R_{et} is calculated by using a Gamry Echem Analyst with an equivalent circuit shown in Fig. S7. R_{et} increases from 6.4 Ω, 8.5 Ω, 10.2 Ω–12.3 Ω for the strain of 0%, 50%, 100% and 150%, respectively. It can be speculated that, by extending of the bionic sensor, the fully folded surface gradually unfolded, as illustrated in Fig. 4A of the inset graph, the increase of the resistance may attribute to the reduce of the conductive path between the wrinkles. The above results reflect the bionic sensor exhibits the fast electron transfer property.

To study the effect of the tunable ECSAs on the electrochemical properties of the sensor towards different concentrations of redox probes, CV experiments with ferricyanide redox pair were carried out. The bionic sensor was firstly measured at different strain states (0%, 50%, 100%, and 150%), then 10 stretching/releasing cycles were applied and the CV was measured subsequently at each strain state. As observed in Fig. 4B, the sensor at different strain states exhibits basically unchanged redox peak separations of the ferricyanide redox pair (towards 1 mM $[Fe(CN)_6]^{3-/4-}$), however, their heights of peaks show large stepped increases. After 10 fatigue cycles, the CV curves remain nearly identical at each strain state. The results indicate that the bionic sensor can response to ferricyanide molecules with good electrochemical response and reproducibility. In addition, the sensor exhibits different peaks' current towards the redox at different strain states, which mainly attributes to their differences in the exposed ECSA according to the Cottrell's relation ($i \propto A$, where i is the current and A is the surface area of the electrode). The peaks' current of the bionic sensor increases with a linear proportion to the redox molecules concentrations from 0.1 mM to 10 mM (Fig. 4C and D). As a result, the stretchable bionic sensor possesses different sensitivities at different strain states. The inset graph shown in Fig. 4D demonstrates that their sensitivities exhibit a linear relationship with the strain states of the

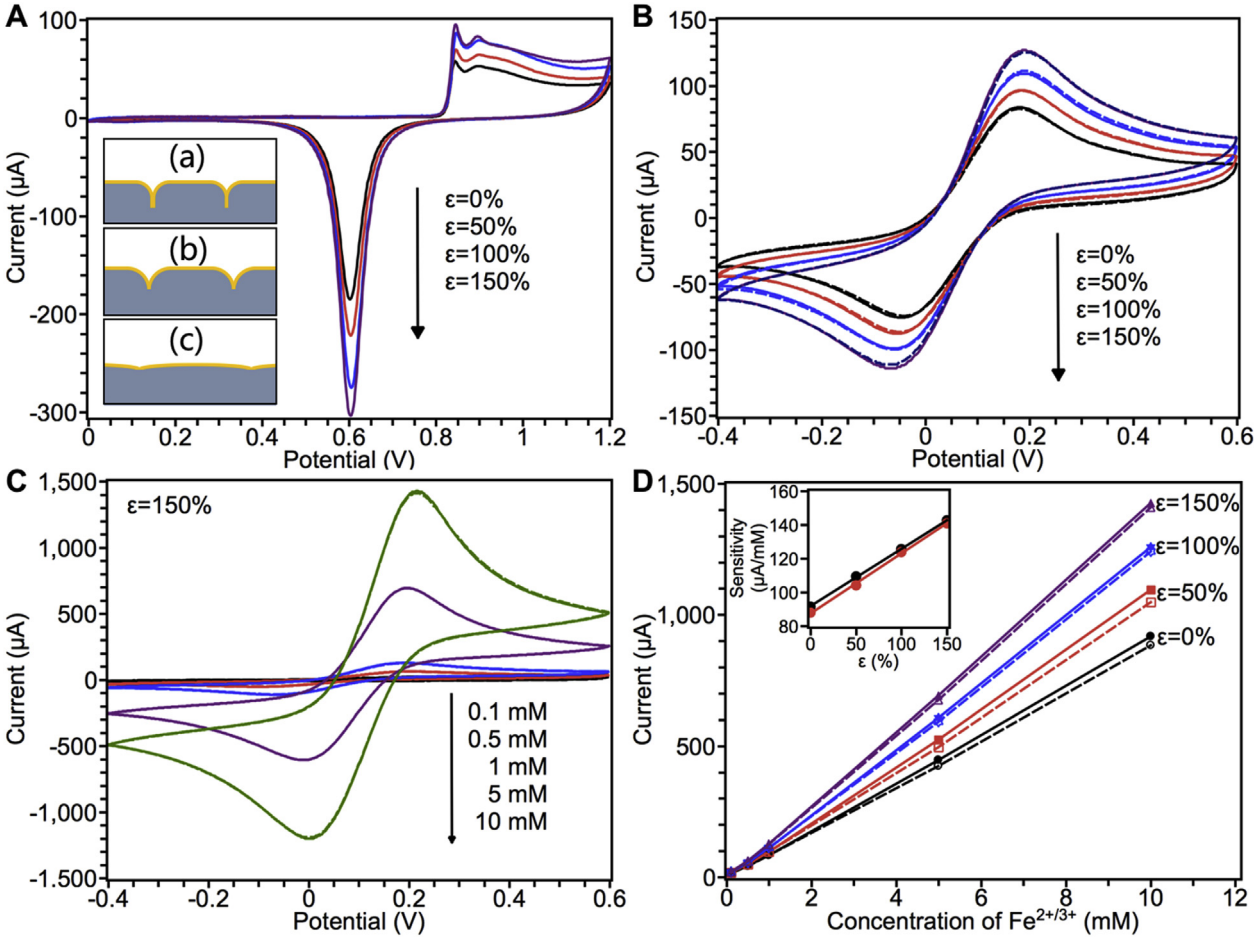

Fig. 4. Electrochemical performances of the stretchable bionic sensor. (A) Cyclic voltammograms (CV) curves of the bionic sensor obtained in 0.5 M H_2SO_4 at different stretching states. The inset illustrations show the surface morphologies with (a) fully folded, (b) partial folded, and (c) unfolded gold membrane of the sensor at different strain states. (B) CV curves of the bionic sensor obtained in 1 mM $[Fe(CN)_6]^{3-/4-}$ at different stretching states, the solid lines refer to the first scan cycle and dotted lines refers to the scans cycle after 10 times stretching/releasing cycles. (C) CV curves of the bionic sensor (at 150% strain state) towards different concentration of $[Fe(CN)_6]^{3-/4-}$. (D) The calibration curves of the bionic sensors towards different concentration of $[Fe(CN)_6]^{3-/4-}$ at different stretching states, the solid lines refer to the first scan cycle and dotted lines refers to the scans cycle after 10 times stretching/releasing cycles. The inset graph shows the calibration curves of the sensor sensitivities at different strain states. (For interpretation of the references to colour in this figure legend, the reader is referred to the Web version of this article.)

bionic sensor, and the sensitivities have a good reproducibility after 10 fatigue cycles as well. Obviously, it can be concluded that the sensitivity of this stretchable bionic sensor can be well controlled by adjusting their extending state (i.e., adjusting their ECSA). Similar to the working principle of a rhinophore, the bionic sensor is in control of its electrochemical surface area (ECSA) changing by regulating the extending/retracting feature. It can be concluded from the SEM images in Fig. 1 and the CV curves in Fig. 4A, during extending of the sensor, the folded membrane gradually unfolded, more surfaces sunken between the ridges are exposed and spread out (illustrations inset in Fig. 4A). According to the Cottrell's relation, a relatively small ECSA exposure can result in low current sensitivity and vice versa. Therefore, programmable sensitivity towards redox molecules can be achieved by extending/retracting the stretchable bionic sensor.

Glucose is utilized as food molecules to mimic the rhinophore bio-inspired tunable sensing function of the stretchable bionic sensor. Gold nanomaterials based electrodes have been widely used as nonenzymatic glucose sensors by direct electro-oxidation of glucose (Dhara and Mahapatra, 2018). They display advantageous electro-catalytic activity towards glucose because of the filled orbitals of gold and the adsorption/electro-adsorption of active species (OH^-) on the surface may participate in the electro-oxidation process; the electrochemical oxidation mechanism has been well studied by numbers of publications (Chen et al., 2013; Hsiao et al., 1996; Zhong et al., 2017). The electro-catalytic activity of the stretchable bionic sensor towards glucose was measured by CV. As shown in Fig. 5A, in the absence of glucose, CV curves of the sensor display the anodic peaks of gold oxide (Au_2O_3) as well as adsorbed active species (AuOH) from 0.4 V to 0.6 V, and the cathodic peaks of the reduction from those oxides at 0.1 V; the current increase from −0.1 V to −0.3 V during the negative scan corresponding to oxygen reduction in the solution. It should be noted that the oxygen reduction currents show an increase with the increases in strain state of the sensor, which attributes to their increase in ECSA can provide more sites for oxygen reaction. When glucose (6 mM) was added, CV responses changed completely due to the glucose electro-oxidation process on the electrode surface. During the positive scan, the anodic current increases significantly with a broad signal composed of two overlapped peaks (at 0.08 V and 0.22 V) and a distinct peak (at 0.54 V). This electro-catalytic behavior including the formation of surface AuOH species, the oxidation of glucose to gluconolactone through AuOH active sites, and followed with the further hydrolyzing the gluconolactone to gluconic acid (Hsiao et al., 1996). Then the anodic peak of glucose oxidation is suppressed by gold oxide formation at more positive potential. In the negative scan, by the reduction of gold oxide and the regeneration of AuOH active sites, a sharp glucose oxidation peak appears at 0.08 V. The sensor at different strain states

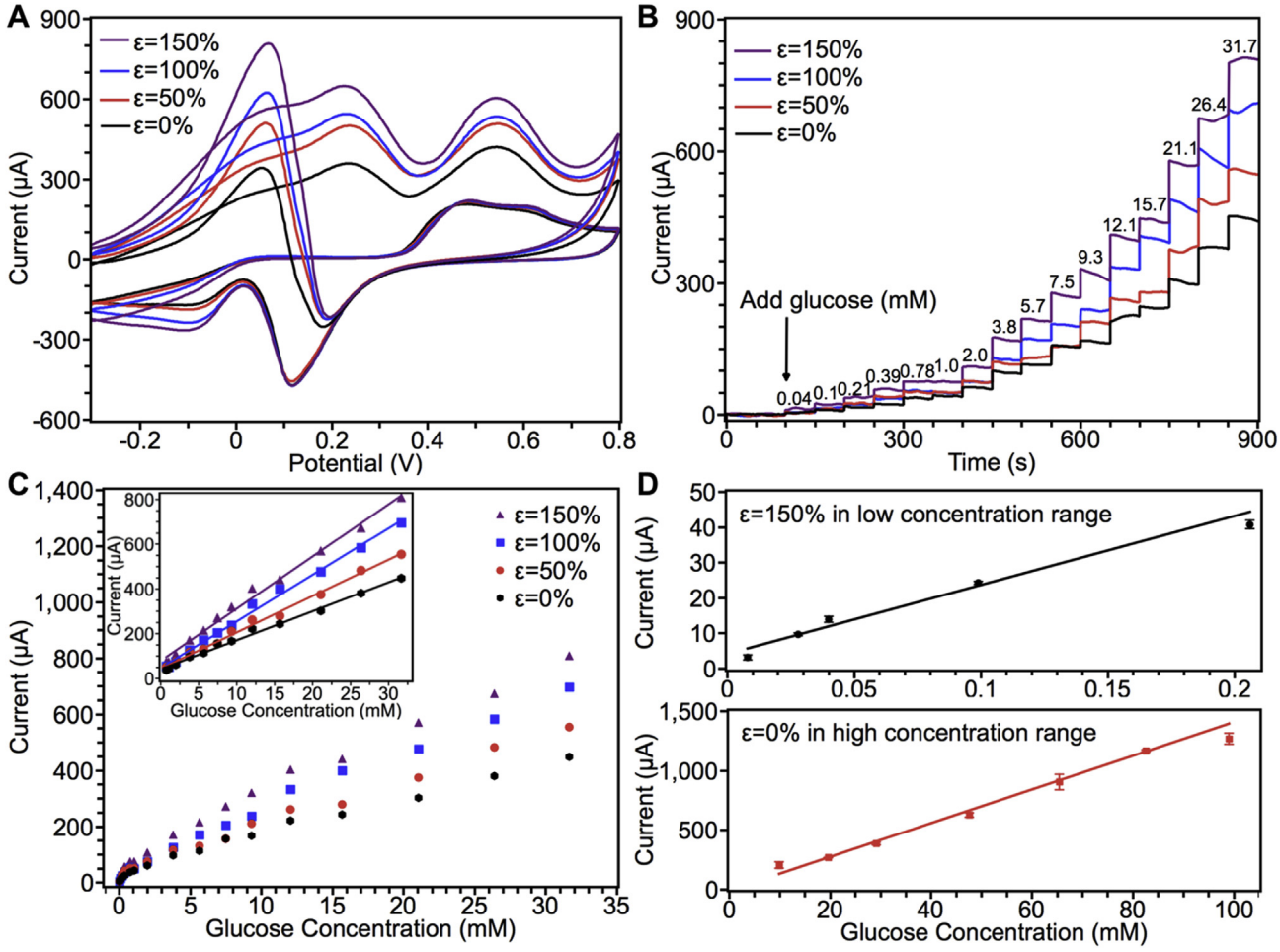

Fig. 5. Electro-catalytic performances of the stretchable bionic sensor. (A) CV (100 mV/s) curves of the bionic sensor at different strain states before (bottom curves) and after (top curves) 6 mM glucose addition. (B) Typical amperometric responses curves of the bionic sensor at different strain states towards the successive injection of different concentrations of glucose at an applied potential of 0.1 V. (C) The calibration curves of the amperometric tests shown in Fig. 4B. Inset graph shows the linear relations in the concentration range from 0.8 to 31.7 mM. (D) The calibration curves of the amperometric tests in the low concentration range from 8 to 206 μM (top graph) and the high concentration range from 10 to 100 mM (bottom graph).

exhibits the same positions of the anodic and cathodic peaks, however, their current intensities increase with the increases in the strain of the sensor from 0% to 150%. It is clear that this stretchable bionic sensor exhibits great electro-catalytic activity towards glucose oxidization. Moreover, their performances can be tuned by adjusting the strain state of the sensor.

Amperometric technique is a powerful approach to continuously and real-time detect chemical molecules with changeable concentrations, which is appropriate to mimic the chemosensory ability of the rhinophore. A proper applied potential is the primary condition for sensitive glucose detection. The amperometric experiments at the applied potential range from 0.05 V to 0.3 V were tested, neither of the potential lower than 0 V nor higher than 0.3 V were employed (to avoid the probable influences from the oxygen, active species and gold oxides). As the results shown in Fig. S8A, an optimum potential at 0.1 V was achieved, which had higher response signal than those from other applied potentials towards various concentrations of glucose. Typical amperometric responses curves are shown in Fig. 5B (applied potential at 0.1 V) of the stretchable bionic sensor at different strain state towards the successive addition of different concentrations of glucose. The currents exhibit the stepped increase with the increment of glucose concentrations. Their calibration curves shown in Fig. 5C demonstrate the good linear relationship between current and glucose concentration for the bionic sensor at all the strain states. The sensitivities are 13.0, 16.3, 20.9 and 23.4 μA mM^{-1} in the concentration range from 0.8 to 31.7 mM for the bionic sensor strain at 0%, 50%, 100% and 150%, respectively. Additionally, the sensitivities exhibit a linear relationship with the strain states of the bionic sensor. Furthermore, the selectivity and the stability of the bionic sensor were characterized. As shown in Fig. S8B, at the applied potential of 0.1 V, the current responses towards ascorbic acid (AA), uric acid (UA) and dopamine (DA) are negligible compared with glucose. Fig. S9 showed the bionic sensor exhibit a proper stability toward glucose in the low and high concentration range. The above results indicate that this stretchable bionic sensor possesses programmable sensitivities towards glucose detection by adjusting its strain state, which vividly mimic the tunable sensory functions of rhinophore by extending/retracting at different length.

Inspired by the smart and multifunctional chemosensory ability of Marine molluscs' rhinophore, including the far/near-field chemical detection and the orientation to food/odor source by extending/retracting its length. The as-prepared stretchable bionic sensor was tested to mimic those functions. As shown in Fig. 5D, the bionic sensor for the detection in a lower glucose concentration range (8 μM–206 μM) is set at 150% strain; as a result, a high sensitivity of 195.4 μA mM^{-1} is achieved. While for the detection in a higher glucose concentration range from 10 mM to 100 mM, the bionic sensor is set at 0% strain; thus, a moderate sensitivity of 14.2 μA mM^{-1} was obtained. This tunable sensitivity is similar to the rhinophore's far/near-field chemical detection mode; i.e., at initiate long-distance search range, which is of lower molecular concentrations that far from the source (as

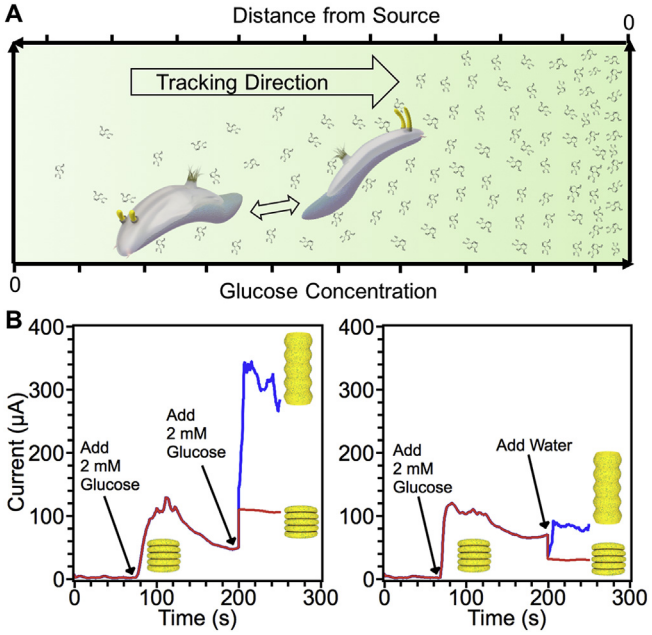

Fig. 6. The conceptual illustration of the molecule tracking mode and the experimental demonstrations by the stretchable bionic sensor. (A) Scheme of the molecule tracking mode for Marine molluscs. (B) The real-time amperometric measurements of the stretchable bionic sensor to mimic the molecular source orientation process.

conceptually illustrated in Fig. 6A), the bionic sensor/rhinophore extend itself to increase the surface area for more sensitive detection; once find the source direction and tracking along the gradually increased molecular concentrations, the bionic sensor/rhinophore will hold at a certain length until near the source. It was also demonstrated by biologists that animals may set a higher concentration response threshold for the molecule (odor) of more abundant food, which can enhance the capturing probability and avoid energy expenditure for little reward (Atema, 2018). This smart biological behavior can also be achieved by the as-prepared stretchable bionic sensor with setting a response threshold for chemical molecules at a certain strain state.

The extending of the rhinophore orientated on the direction of the greatest concentration may be responsible for the orientation to the molecular source (Atema, 2018). It is clear that animals' rhinophores are stretching out with pendulum-like motions during tracking odor source, which suggests the bionic sensor can detect while extending itself for direction searching. A conceptual illustration of the molecule tracking mode of the stretchable bionic sensor/rhinophore is shown in Fig. 6A. In the direction towards odor source, the molecular concentrations are higher; oppositely, the concentrations are lower in the direction away from odor source The real-time amperometric measurements of the stretchable bionic sensor was carried out with the custom-designed cell which allows the electrochemical detecting while extending the sensor (Fig. S6). As shown in Fig. 6B, the bionic sensor is at 0% strain state, 2 mM glucose was added firstly, the response signal gradually increased and afterwards decreased to a steady current due to the diffusion behavior of a stream of molecules with a large concentration range and gradient. Then, 2 mM glucose was added, the amperometric measurements was temporarily stopped for 2 min, so that the glucose could diffuse with a homogeneous solution to mimic the bionic sensor stretch into a higher concentration region. The bionic sensor continued to detect while extending its length, and a dramatic current increase was achieved. In contrast, when the bionic sensor detected without extending its length, its current increment was almost 4 times lower than that of the extending sensor. To mimic the bionic sensor that stretches into the direction away from odor source, water was added in order to dilute the glucose concentration, and the bionic sensor detected with extending its length showed a decrease followed with a small increased current, while the bionic sensor detected without extending showed a stepped decrement. Obviously, the response signals during sensor's extending are largely enhanced, and the orientation to different concentration regions has apparently been distinguished via these two cases.

4. Conclusion

In conclusion, a bio-inspired highly stretchable electrochemical glucose sensor with programmable sensing performance was demonstrated. By vividly mimicking the anatomical units and the extending/retracting features of a rhinophore, the as-proposed bionic sensor possesses a highly stretchable feature with the buckled gold nanomembrane. As a result, the bionic sensor can regulate the ECSA and achieve a programmable sensitivity towards glucose detection by controlling its extending and retracting state. In addition, the bionic sensor was demonstrated by mimicking the sensing functions of the rhinophore, including a far/near-field chemical detection and orientation to the targeted molecular source direction. Overall, this bionic sensor presents a novel sensing concept, which will be advantageous for future development of smart systems such as wearable devices, soft robotics and bionics devices.

Declaration of competing interest

The authors declare that they have no known competing financial interests or personal relationships that could have appeared to influence the work reported in this paper.

CRediT authorship contribution statement

Shuqi Wang: Conceptualization, Investigation, Methodology, Formal analysis, Writing - original draft. **Chunyan Qu:** Software. **Lin Liu:** Writing - review & editing. **Lianhui Li:** Writing - review & editing. **Tie Li:** Funding acquisition. **Sujie Qin:** Writing - review & editing. **Ting Zhang:** Supervision, Funding acquisition, Writing - review & editing.

Acknowledgements

This work was supported by the National Key R&D Program of China (2017YFA0701101, 2018YFB1304700), the National Natural Science Foundation of China (61574163, 61801473, 51702354) and the Science Foundation for Distinguished Young Scholars of Jiangsu Province, China (BK20170008).

Appendix A. Supplementary data

Supplementary data to this article can be found online at https://doi.org/10.1016/j.bios.2019.111519.

References

Abellán-Llobregat, A., Jeerapan, I., Bandodkar, A., Vidal, L., Canals, A., Wang, J., Morallón, E., 2017. Biosens. Bioelectron. 91, 885–891.
Atema, J., 2018. Bull. Mar. Sci. 94 (3), 479–516.
Bandodkar, A.J., Jeerapan, I., Wang, J., 2016a. ACS Sens. 1 (5), 464–482.
Bandodkar, A.J., Jeerapan, I., You, J.-M., Nunez-Flores, R., Wang, J., 2016b. Nano Lett. 16 (1), 721–727.
Bandodkar, A.J., Nuñez-Flores, R., Jia, W., Wang, J., 2015. Adv. Mater. 27 (19), 3060–3065.
Basil, J.A., Bahctinova, I., Kuroiwa, K., Lee, N., Mims, D., Preis, M., Soucier, C., 2005. Mar. Freshw. Behav. Physiol. 38 (3), 209–221.
Basil, J.A., Hanlon, R.T., Sheikh, S.I., Atema, J., 2000. J. Exp. Biol. 203 (9), 1409–1414.
Cai, P.Q., Leow, W.R., Wang, X.Y., Wu, Y.L., Chen, X.D., 2017. Adv. Mater. 29 (26), 1605529.
Chen, C., Xie, Q.J., Yang, D.W., Xiao, H.L., Fu, Y.C., Tan, Y.M., Yao, S.Z., 2013. RSC Adv. 3 (14), 4473–4491.

Chen, Y.C., Cai, H., Chen, Z.L., Feng, Q.L., 2017. Build. Environ. 118, 101–112.
Cummins, S.F., Erpenbeck, D., Zou, Z., Claudianos, C., Moroz, L.L., Nagle, G.T., Degnan, B.M., 2009. BMC Biol. 7 (1), 28.
Dhara, K., Mahapatra, D.R., 2018. Microchim. Acta 185 (1), 49.
Heikenfeld, J., Jajack, A., Rogers, J., Gutruf, P., Tian, L., Pan, T., Li, R., Khine, M., Kim, J., Wang, J., Kim, J., 2018. Lab Chip 18 (2), 217–248.
Hsiao, M.W., Adzic, R.R., Yeager, E.B., 1996. J. Electrochem. Soc. 143 (3), 759–767.
Jiang, D.W., Liu, Z.S., Wu, K.K., Mou, L.L., Ovalle-Robles, R., Inoue, K., Zhang, Y., Yuan, N.Y., Ding, J.N., Qiu, J.H., Huang, Y., Liu, Z.F., 2018. Polymers 10 (4), 375.
Kang, D., Pikhitsa, P.V., Choi, Y.W., Lee, C., Shin, S.S., Piao, L.F., Park, B., Suh, K.Y., Kim, T.I., Choi, M., 2014. Nature 516 (7530), 222–226.
Kim, D.H., Lu, N.S., Ma, R., Kim, Y.S., Kim, R.H., Wang, S.D., Wu, J., Won, S.M., Tao, H., Islam, A., Yu, K.J., Kim, T.I., Chowdhury, R., Ying, M., Xu, L.Z., Li, M., Chung, H.J., Keum, H., McCormick, M., Liu, P., Zhang, Y.W., Omenetto, F.G., Huang, Y.G., Coleman, T., Rogers, J.A., 2011. Science 333 (6044), 838–843.
Lee, H., Choi, T.K., Lee, Y.B., Cho, H.R., Ghaffari, R., Wang, L., Choi, H.J., Chung, T.D., Lu, N., Hyeon, T., Choi, S.H., Kim, D.H., 2016. Nat. Nanotechnol. 11, 566–572.
Lee, Y.K., Jang, K.-I., Ma, Y., Koh, A., Chen, H., Jung, H.N., Kim, Y., Kwak, J.W., Wang, L., Xue, Y., Yang, Y., Tian, W., Jiang, Y., Zhang, Y., Feng, X., Huang, Y., Rogers, J.A., 2017. Adv. Funct. Mater. 27 (9), 1605476.
Liu, Y.L., Jin, Z.H., Liu, Y.H., Hu, X.B., Qin, Y., Xu, J.Q., Fan, C.F., Huang, W.H., 2016. Angew. Chem. Int. Ed. 55 (14), 4537–4541.
Liu, Y.L., Qin, Y., Jin, Z.H., Hu, X.B., Chen, M.M., Liu, R., Amatore, C., Huang, W.H., 2017. Angew. Chem. Int. Ed. 56 (32), 9454–9458.
Qi, D., Liu, Z., Yu, M., Liu, Y., Tang, Y., Lv, J., Li, Y., Wei, J., Liedberg, B., Yu, Z., Chen, X., 2015. Adv. Mater. 27 (20), 3145–3151.
Ristic, B., Angley, D., Moran, B., Palmer, J.L., 2017. Sensors 17 (4), 918.
Rogers, J.A., 2017. Nat. Nanotechnol. 12 (9), 839–840.
Ruth, P., Schmidtberg, H., Westermann, B., Schipp, R., 2002. J. Morphol. 251 (3), 239–255.
Wang, X.W., Liu, Z., Zhang, T., 2017. Small 13 (25), 1602790.
Windmiller, J.R., Wang, J., 2013. Electroanalysis 25 (1), 29–46.
Yang, Y., Gao, W., 2018. Chem. Soc. Rev. 48, 1465–1491.
Yang, Z.Y., Sassa, F., Hayashi, K., 2018. ACS Sens. 3 (6), 1174–1181.
Zhong, S.-L., Zhuang, J., Yang, D.-P., Tang, D., 2017. Biosens. Bioelectron. 96, 26–32.
Zhu, Y.J., Moran-Mirabal, J., 2016. Adv. Electron. Mater. 2 (3), 1500345.